Available online at www.sciencedirect.com
ScienceDirect
Flow Measurement and Instrumentation 18 (2007) 139–147
Flow Measurement and Instrumentation
www.elsevier.com/locate/flowmeasinst

An image analysis technique for the study of gas–liquid slug flow along vertical pipes — associated uncertainty

T.S. Mayor, A.M.F.R. Pinto, J.B.L.M. Campos*

Centro de Estudos de Fenómenos de Transporte, Departamento de Engenharia Química, Faculdade de Engenharia da Universidade do Porto, Rua Dr. Roberto Frias, 4200-465 Porto, Portugal

Received 9 June 2006; accepted 20 December 2006

Abstract

An image analysis technique for the study of continuous co-current gas–liquid slug flow, in vertical columns, is reported. The technique comprises the automatic analysis of a sequence of video frames with the purpose of object (bubbles) tracking and characterization (dimension, velocity, distance). Its applicability to continuous slug flow conditions (even for very large number of bubbles) and the high accuracy of the results are the main added value of the proposed technique. The evaluation of the uncertainty associated with the parameters measured is performed (following the *general uncertainty analysis approach*). Partial uncertainties are acknowledged in bubble boundary definition, time measurement and calibration procedure. Expressions are derived for the computation of the overall uncertainty of bubble velocity, bubble length and liquid slug length. Global relative uncertainties of 5%, 2.5% and 7%, were found, for these parameters. The uncertainty estimation supports the ongoing trend for the implementation of image analysis techniques for the study of slug flow patterns.

Keywords: Flow visualization; Image analysis; Error analysis; Uncertainty evaluation; Two-phase flow; Slug flow; Bubble columns

1. Introduction

The implementation of image analysis techniques for the study of phenomena is spanning over different fields of research, as a natural consequence of its non-intrusiveness, but also a development promoted by the exponential evolution of hardware and software applications. Two-phase and multiphase flows are examples of areas that have profited with the emergence of these techniques. Two-phase slug flow experiments, for instance, is a potential field of application for these new visualization strategies.

Slug flow studies have been performed using several experimental techniques, with more or less intrusive approaches (as in Pinto et al. [1] or Van Hout et al. [2], just to mention some, featuring pressure probes and optical fibre probes, respectively). Non-intrusive approaches have also been reported. Hasanein et al. [3] describe a visualization technique based on video recordings of the flow (with bubble length estimation achieved by direct comparison with on site rulers), whereas Polonsky et al. [4] mention an image processing procedure for the study of the motion of individual Taylor bubbles. Moreover, Van Hout et al. [5] report the application of the latter technique to continuous slug flow (although applicable only to a small number of bubbles). An experimental technique based on laser diodes and photo cells is also proposed [6] as a tool for the study of the motion of individual Taylor bubbles. Although non-intrusive, this technique is not suitable for continuous slug flow conditions.

Gaining more and more adepts in the fluid mechanics research community, the image analysis techniques are providing solutions to tackle the experimental study of slug flow. To support this ongoing trend, a detailed evaluation of the uncertainty associated with this measurement technique is needed.

The main goal of this work is to provide information concerning a straightforward and accurate image analysis technique, developed specially for the study of continuous gas–liquid slug flow, in vertical columns, and applicable for the measurement of a large number of bubbles (several thousands). Detailed assessment of the uncertainty associated with the parameters measured by this technique is performed. Focus is

* Corresponding author. Fax: +351 225081449.
E-mail address: jmc@fe.up.pt (J.B.L.M. Campos).

0955-5986/$ - see front matter © 2007 Elsevier Ltd. All rights reserved.
doi:10.1016/j.flowmeasinst.2007.05.004

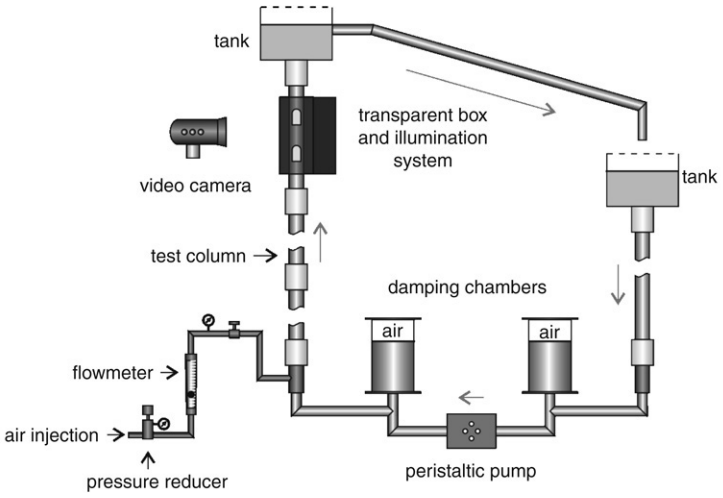

Fig. 1. Experimental set-up.

put on the propagation of the uncertainty of each measured variable over the total uncertainty of typical flow parameters (bubble velocity, bubble length and liquid slug length).

2. Experimental set-up

The experimental apparatus is shown schematically in Fig. 1. Experiments were performed in an acrylic vertical column (6.5 m long). Water was used as flowing medium. The flow was set and controlled by a peristaltic pump with damping chambers placed at the pump inlet and outlet to assure a continuous flow. A large open tank with a lateral outlet was mounted at the top of the pipe to minimise free-surface oscillations. The liquid flow rate was measured at the outlet of the tank, before and after each experiment. The liquid temperature was measured by a thermocouple placed inside the tank. Air from a pressure line was introduced laterally at the base of the column through a 3 mm internal diameter injector. The air flow rate was measured by calibrated rotameters.

Images of slug flow around the vertical coordinate 5.4 m (from the base of the column) were recorded using a Canon digital video camcorder (model XM1) operating at a frequency of 25 Hz. A rectangular transparent acrylic box (1.2 m long) filled with water was fitted to the column at the measuring sections, in order to reduce image distortion and heating effects from the light source (Fig. 2).

Uniform illumination over the whole test section was achieved by means of an illumination system as illustrated in Fig. 2(a). Two fluorescent lamps, equipped with an electronic ballast to avoid light scintillation problems (boosting scintillation frequencies to the kHz range), were mounted inside an opaque box with a diffusive surface in front of the lamps for greater light uniformity. The illumination kit was placed in contact with the transparent acrylic box as illustrated in Fig. 2(b). Both lateral faces as well as top and bottom sides of the acrylic box were covered with an opaque material in order to assure a single light source illuminating the column test-section.

Very short exposure times were chosen to assure "frozen" snapshots. Auto-focus was used to infer an adequate focal

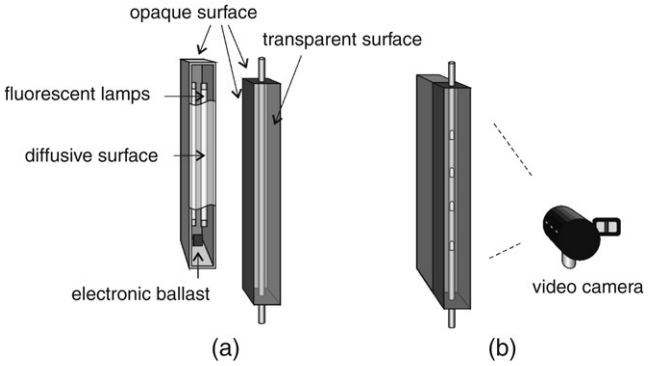

Fig. 2. Schematic representation of the illumination system.

length for each experimental condition, followed by steady manual focus during the experiments. This procedure avoided running the auto-tracking focus of the camera auto-focus system, whenever bubbles appeared in the field of view. A 90° rotation of the camera was chosen for better pixel resolution in the vertical coordinate, which is the main flow direction (the non-rotated camera field of view is 720 (width) × 576 (height) pixels). Different camera focal lengths were used according to the flow complexity and the average bubble and liquid slug dimensions (longer bubbles require a smaller image magnification whilst a more complex flow pattern calls for a larger magnification). Depending on the aforementioned balance, up to 0.6 m of pipe were captured in the camera field of view.

3. Video processing — the image analysis

The recorded videos were transferred to a personal computer hard drive using video editing software (Adobe Premiere). Raw videos were stored in the original acquired format (Microsoft DV) for further processing. For the sake of hard drive capacity, audio information was discarded in the videos. Moreover, from the total field of view only the strip containing the test column was extracted and further processed (Fig. 3). This resulted in a considerable reduction in the size of the stored files as well as processing time. Each video strip was processed using

Fig. 3. Experimental frame: (a) full frame; (b) strip of frame.

a MATLAB code specially developed for the purpose. The choice of MATLAB environment as a video processing tool led to choosing Microsoft AVI codification for the output video format of the strips, since it is the only video format directly readable by MATLAB internal routines.

Notice that in Microsoft AVI format, a 30 min video strip corresponds to about 4 GB of hard drive space. Considering that the direct analysis of such videos would cause RAM (random access memory) shortness problems, an extra step was implemented, before the video analysis, in order to further decrease the digital size of the videos: each video strip was split into 70 consecutive video files, using a general video tool together with automation Macro software.

Each of these shorter video files was loaded into the MATLAB workspace as a sequence of frames. Each frame corresponds to a snapshot of the camera field of view (a frame at each 0.04 s, corresponding to a frequency of 25 Hz). A sequential procedure was implemented for processing each image frame. The outcome of every step of the procedure is shown in the images of Fig. 4, and briefly described below.

3.1. Image loading

Each frame was loaded as 8 bits RGB (red, green and blue) colour format (Fig. 4(a)).

3.2. Image conversion

Each frame was converted from RGB to greyscale mode (Fig. 4(b)). The output image has 256 grey levels, ranging from 0 (black) to 255 (white). A greyscale version of the background image was also prepared. This background image is used for image contrast enhancements.

3.3. Image contrast enhancement

The subtraction of the background image (corresponding to a snapshot of the column with stagnant liquid and no gas flow) from the continuous flow image (with both liquid and gas) enhances the image contrast. This procedure eliminates any information (or colour change) not related to the gas phase. The resulting image is shown in Fig. 4(c).

3.4. Image filtering

In order to remove or attenuate the image noise, a median filter was applied to the image (Fig. 4(d)). In this procedure, every pixel of the image is substituted by the median of its neighbour pixels. As a result, any eventual pixel outliers, i.e., pixels diverging considerably from the surrounding ones, are discarded. A slight decrease in image sharpness occurs.

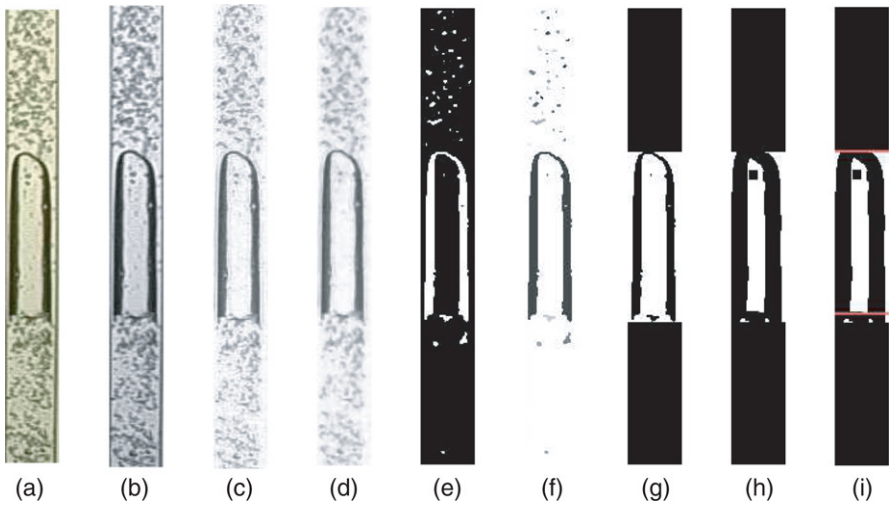

Fig. 4. Sequential steps in the image process: (a) RGB image; (b) greyscale image; (c) after background subtraction; (d) after median filter; (e) after inversion and conversion to binary mode; (f) after labelling; (g) after object analysis; (h) after erosion; (i) bubble boundaries. (For interpretation of the references to colour in this figure legend, the reader is referred to the web version of this article.)

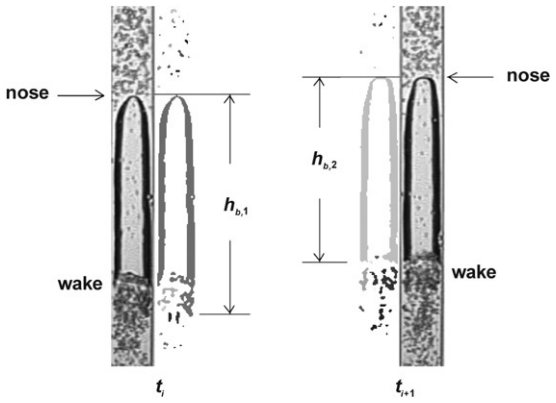

Fig. 5. Representation of consecutive bubble images, with bubble boundaries based on simple object lengths.

3.5. Image conversion to binary mode

Conversion of a greyscale image to binary mode consists in a reduction to two of the number of grey levels of the original image: one corresponding to black (0) and another corresponding to white (1). This is accomplished by means of a threshold value, i.e., a pixel value (or luminosity) defining the transition between black and white colours. Once the threshold value (reference luminosity) is defined, an image simplification takes place: all pixels with luminosity values lower than the threshold value are considered black, while the remaining pixels are considered white. This operation creates images like the one depicted in Fig. 4(e). In most experiments, a threshold value of 0.35 was used. See Appendix for further details on the threshold value.

3.6. Image objects labelling

The above procedure created a black and white image that can be understood as a black background with white objects in the foreground. These white objects were labelled using different grey levels to allow for easier observation of their positioning and dimensions (Fig. 4(f)).

3.7. Object analysis I — bubble nose definition

The objects in the image, easily perceived in the labelled representation (Fig. 4(f)), can be described in terms of their dimensions (width, length), their white area (estimative of the area of the white pixels), their square area (area of the smallest square comprising the object), etc. Each of these descriptions allows different analysis of the objects.

The aim of the algorithm is the tracking of Taylor bubbles moving upwards in a flowing liquid. As depicted in Fig. 4, Taylor bubbles flow through more or less aerated liquid slugs, depending on the liquid physical properties, gas–liquid flow rates, column diameter, etc. In order to distinguish between Taylor bubbles and small bubbles flowing in the liquid slug, the length of the objects in the image was used as a sorting parameter. For this purpose, a minimum bubble length was defined to acknowledge the presence of Taylor bubbles. Depending on the flow complexity and average bubble length, a minimum bubble length ranging from $1D$ to $3D$ was used throughout the analysis of all experiments.

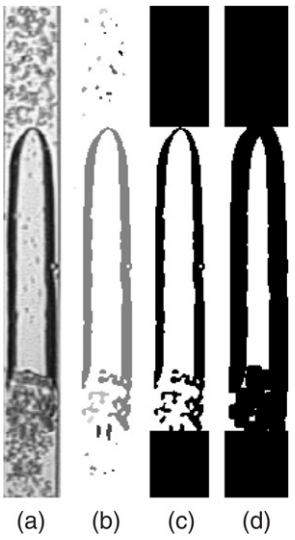

Fig. 6. (a) Greyscale image; (b) labelled version; (c) binary version and (d) binary eroded version.

The use of object length as a sorting parameter allowed immediate definition of the Taylor bubble nose as well as a rough estimate of the position of the Taylor bubble rear. This uncertainty is due to oscillations in the bubble rear as Taylor bubbles flow in a column, and to the small bubbles travelling in the liquid wake. If bubble rear positioning was based on objects length, bubble length values would change considerably from frame to frame. Fig. 5 illustrates this problem. There is an obvious difference in the bubble length in consecutive frames.

3.8. Image "erosion"

Image erosion is a morphological image operation that changes every pixel in an image according to the values of its neighbouring pixels. More specifically, image erosion sets the value of every pixel in an image to the minimum value of its surrounding pixels. Thus, when a binary image (black and white pixels) undergoes erosion, there is a decrease in the area of the objects (in white), since some white pixels in the extremity of the objects are set to black (minimum value of the surrounding pixels). This change in the area of the objects is easily recognised in Fig. 6(d).

A MATLAB internal function ('*strel*') was applied to define the surrounding area used for image erosion purposes. A flat, disk-shaped structuring element was used (type '*disk*'), with a 4 pixel radius. More details on this function can be found in [7].

3.9. Object analysis II — bubble rear definition

The erosion of the white objects allowed to isolate the central white object (Fig. 6(d)), previously blended with small objects in the bubble wake region. Notice that this object can easily be sorted from the remaining objects since it clearly has the largest white area. Analysing this central eroded object in detail, it can be seen that its lowest white pixel (at the base of the object)

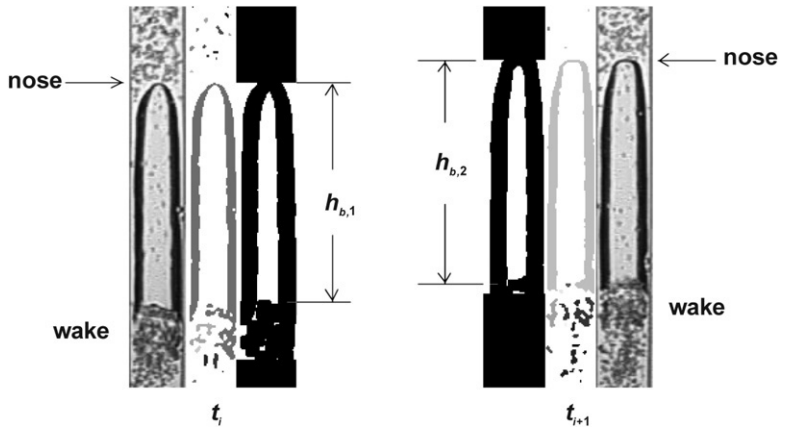

Fig. 7. Representation of consecutive bubble images, with bubble boundaries based on object lengths and central area.

matches the beginning of the bubble wake region. Moreover, the upward movement, from frame to frame, of this lowest white pixel is noticeably smooth in comparison to the movement of the lowest white pixel of the central non-eroded object (Fig. 6(b)). This indicates that by defining more accurately the position of the bubble wake region, the erosion procedure enables the acquisition of more robust and coherent bubble length values (discarding the wake region). Fig. 7 depicts this approach.

4. Video processing — the data analysis

By determining the positioning and dimension of Taylor bubbles grabbed in every video frame it is possible to compile information about the flow pattern in slug flow experiments. Two different studies can be performed: one describing the flow pattern at a fixed column position (fixed-point data analysis), and another focussing on the bubble-to-bubble interaction as bubbles move along the column (moving-point data analysis).

4.1. Fixed-point data analysis

Fig. 8 depicts the camera's field of view in a slug flow experiment. Two imaginary reference lines, corresponding to 25% and 75% of the field of view height, were drawn (references 1 and 2, respectively). Bubbles are recognized when their noses cross the upper reference line.

If $t_{1,i}$ and $t_{2,i}$ represent consecutive instants, prior and subsequent, respectively, to the passage of the nose of bubble i, through the upper reference line, the bubble velocity, U_i, is given by:

$$U_i = \frac{z_{\text{nose},i}^{t_{2,i}} - z_{\text{nose},i}^{t_{1,i}}}{t_{2,i} - t_{1,i}} \tag{1}$$

where $z_{\text{nose},i}$ refers to the vertical coordinate of the bubble nose (measured from the base of the camera field of view). The bubble length is obtained directly from the position of its boundaries (nose and rear):

$$h_{b,i} = z_{\text{nose},i}^{t_{2,i}} - z_{\text{rear},i}^{t_{2,i}} \tag{2}$$

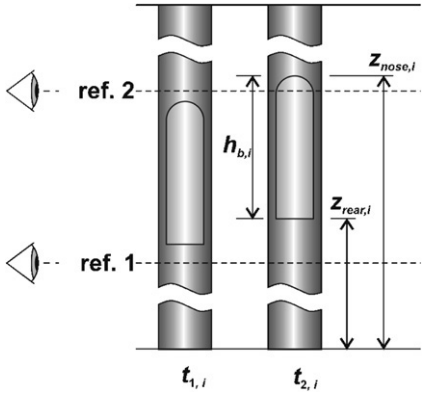

Fig. 8. Representation of the camera field of view in fixed-point analysis, during the passage of a Taylor bubble.

The liquid slug length ahead of bubble i, $h_{s,i-1}$, is computed from the coordinate of the rear of the previous bubble (bubble $i-1$) and the coordinate of the nose of bubble i:

$$h_{s,i-1} = z_{\text{rear},i-1}^{t_{2,i}} - z_{\text{nose},i}^{t_{2,i}} \tag{3}$$

The coordinate of the rear of bubble $i-1$, at instant $t_{2,i}$, can be predicted by:

$$z_{\text{rear},i-1}^{t_{2,i}} = z_{\text{nose},i-1}^{t_{2,i-1}} + (t_{2,i} - t_{2,i-1})U_{i-1}^{t_{2,i-1}} - h_{b,i-1} \tag{4}$$

where $t_{2,i-1}$ refers to the instant at which the nose of bubble $i-1$ crossed the upper reference line. In the above prediction, it is assumed that bubble $i-1$ has constant upward velocity between instants $t_{2,i-1}$ and $t_{2,i}$. This assumption is reasonable unless the bubble is coalescing, interacting or instantly accelerating or decelerating by the time it passes the upper reference line.

The above procedure must be implemented for each video frame to gather information about the characteristics of every bubble (regarding bubble length, velocity and liquid slug length).

All variables referred to above have pixel units (or pixel/s in the velocity case). To accomplish their conversion to real length units, the following correction must be computed:

$$\text{variable [m or m/s]} = \text{variable}\left[\text{pixel or pixel/s}\right]\frac{h_{\text{cal.},m}}{h_{\text{cal.,px}}} \tag{5}$$

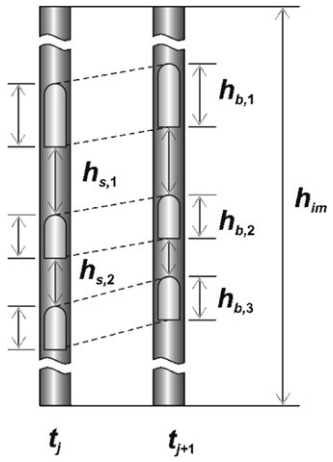

Fig. 9. Representation of camera field of view in moving-point analysis.

where $h_{\text{cal.},m}$ and $h_{\text{cal.,px}}$ refer to the height of the calibration element in metres and pixels units, respectively.

4.2. Moving-point data analysis

In the moving-point data analysis, the focus is put on the bubble-to-bubble interaction. Hence, for higher accuracy, it is important to use an image magnification in which more than one Taylor bubble is visible in the camera field of view. In this scenario, the relation between the bubble velocity and the liquid slug length ahead of the bubble is achieved without using predictions to compute the positioning of bubble boundaries, as in the previous section. Fig. 9 depicts this situation.

Consecutive instants t_j and t_{j+1} are chosen considering the requirement of frames with equal number of bubbles, and with all bubble boundaries inside the camera field of view (no bubbles entering or exiting the field of view).

Bubble velocities are calculated using the following equation, identical to Eq. (1), for every bubble in the chosen frames:

$$U_i = \frac{z_{\text{nose},i}^{t_{j+1}} - z_{\text{nose},i}^{t_j}}{t_{j+1} - t_j} \tag{6}$$

Bubble and liquid slug lengths are computed using the following equations:

$$h_{b,i} = z_{\text{nose},i} - z_{\text{rear},i} \tag{7}$$

$$h_{s,i-1} = z_{\text{rear},i-1} - z_{\text{nose},i} \tag{8}$$

Notice that, for n bubbles in a frame, only $n-1$ liquid slugs are computed. Additionally, the last two equations are applied to each pair of consecutive frames and, therefore, average values for each bubble and liquid slug length are calculated (from every two consecutive frames).

As referred to in the previous section, a correction must be computed to convert the aforementioned variables to real length (or velocity) units (see Eq. (5)).

5. Video processing — the error analysis

The methodology described in the previous sections allows the gathering of information on the variation of the positioning of bubble boundaries along time, which can be transformed into data about velocity of bubbles, length of bubbles and length of liquid slugs. Considering that the acquisition of the initial data (positioning of bubble nose and rear and the time interval between consecutive frames) is accomplished within the precision limits of the equipment used in the process, it is interesting to assess how these uncertainties propagate through the algebraic transformations, required for computing the final variables.

Consider a general parameter Y computed algebraically by a function (the reduction equation) of n measured variables $(y_1, \ldots, y_n)$:

$$Y = f(y_1, y_2, \ldots, y_n) \tag{9}$$

If the uncertainty of each of the measured variables is represented by $\delta y_1, \ldots, \delta y_n$, one can evaluate the uncertainty of parameter Y as follows (*general uncertainty analysis approach*):

$$(\delta Y)^2 = \left(\frac{\partial Y}{\partial y_1}\delta y_1\right)^2 + \left(\frac{\partial Y}{\partial y_2}\delta y_2\right)^2 + \cdots + \left(\frac{\partial Y}{\partial y_n}\delta y_n\right)^2 \tag{10}$$

The evaluation of the uncertainty of some slug flow parameters is described in detail in the following sections. Focus is put on the procedure *fixed-point data analysis* (Section 4.1), as it has, from the aforementioned two, the higher associated uncertainty (it requires the prediction of the positioning of bubble boundaries (Eq. (4)).

5.1. Bubble velocity

The velocity of the bubbles passing a certain vertical coordinate (reference line) can be computed using Eq. (1), after rearranging according to Eq. (5):

$$U_i = \frac{z_{\text{nose},i}^{t_{2,i}} - z_{\text{nose},i}^{t_{1,i}}}{t_{2,i} - t_{1,i}} \frac{h_{\text{cal.},m}}{h_{\text{cal.,px}}}$$

$$\Leftrightarrow U = \frac{z_{\text{nose},i}^{t_{2,i}} - z_{\text{nose},i}^{t_{1,i}}}{\Delta t} \frac{h_{\text{cal.},m}}{h_{\text{cal.,px}}} \tag{11}$$

According to the *general uncertainty analysis approach*, the uncertainty of the resulting variable (U) can be calculated as follows:

$$(\delta U)^2 = \left(\frac{\partial U}{\partial z_{\text{nose}}^{t_{2,i}}}\delta z_{\text{nose}}^{t_{2,i}}\right)^2 + \left(\frac{\partial U}{\partial z_{\text{nose}}^{t_{1,i}}}\delta z_{\text{nose}}^{t_{1,i}}\right)^2 + \left(\frac{\partial U}{\partial \Delta t}\delta \Delta t\right)^2 + \left(\frac{\partial U}{\partial h_{\text{cal.},m}}\delta h_{\text{cal.},m}\right)^2 + \left(\frac{\partial U}{\partial h_{\text{cal.,px}}}\delta h_{\text{cal.,px}}\right)^2 \tag{12}$$

where $\delta z_{\text{nose}}^{t_{1,i}}$, $\delta z_{\text{nose}}^{t_{2,i}}$, $\delta \Delta t$, $\delta h_{\text{cal.},m}$ and $\delta h_{\text{cal.,px}}$ refer to the uncertainties of the corresponding measured variables. The five partial derivatives are expanded in the following equations.

Notice that both sides of each expanded equation were divided by the variable U or by its corresponding ratio (according to the reduction equation).

$$\left(\frac{1}{U}\right)\frac{\partial U}{\partial z_{\text{nose}}^{t_{2,i}}} = \left(\frac{\Delta t}{z_{\text{nose},i}^{t_{2,i}} - z_{\text{nose},i}^{t_{1,i}}}\frac{h_{\text{cal.,px}}}{h_{\text{cal.},m}}\right)\frac{1}{\Delta t} = \frac{1}{\Delta z_{\text{nose}}} \tag{13}$$

$$\left(\frac{1}{U}\right)\frac{\partial U}{\partial z_{\text{nose}}^{t_{1,i}}} = \left(\frac{\Delta t}{z_{\text{nose},i}^{t_{2,i}} - z_{\text{nose},i}^{t_{1,i}}}\frac{h_{\text{cal.,px}}}{h_{\text{cal.},m}}\right)\frac{-1}{\Delta t} = \frac{-1}{\Delta z_{\text{nose}}} \tag{14}$$

$$\left(\frac{1}{U}\right)\frac{\partial U}{\partial \Delta t} = \left(\frac{\Delta t}{z_{\text{nose},i}^{t_{2,i}} - z_{\text{nose},i}^{t_{1,i}}}\frac{h_{\text{cal.,px}}}{h_{\text{cal.},m}}\right) \times \frac{-(z_{\text{nose},i}^{t_{2,i}} - z_{\text{nose},i}^{t_{1,i}})}{\Delta t^2} = \frac{-1}{\Delta t} \tag{15}$$

$$\left(\frac{1}{U}\right)\frac{\partial U}{\partial h_{\text{cal.},m}} = \left(\frac{\Delta t}{z_{\text{nose},i}^{t_{2,i}} - z_{\text{nose},i}^{t_{1,i}}}\frac{h_{\text{cal.,px}}}{h_{\text{cal.},m}}\right) \times \frac{(z_{\text{nose},i}^{t_{2,i}} - z_{\text{nose},i}^{t_{1,i}})}{\Delta t h_{\text{cal.,px}}} = \frac{1}{h_{\text{cal.},m}} \tag{16}$$

$$\left(\frac{1}{U}\right)\frac{\partial U}{\partial h_{\text{cal.,px}}} = \left(\frac{\Delta t}{z_{\text{nose},i}^{t_{2,i}} - z_{\text{nose},i}^{t_{1,i}}}\frac{h_{\text{cal.,px}}}{h_{\text{cal.},m}}\right) \times \frac{-(z_{\text{nose},i}^{t_{2,i}} - z_{\text{nose},i}^{t_{1,i}})h_{\text{cal.},m}}{\Delta t (h_{\text{cal.,px}})^2} = \frac{-1}{h_{\text{cal.,px}}} \tag{17}$$

where Δz_{nose} is the pixel displacement of the nose of the bubble, between the consecutive instants t_1 and t_2 (when the bubble passes the upper reference line). Eq. (12) can, thus, be rewritten in the form

$$\left(\frac{\delta U}{U}\right)^2 = \left(\frac{\delta z_{\text{nose}}^{t_{2,i}}}{\Delta z_{\text{nose}}}\right)^2 + \left(-\frac{\delta z_{\text{nose}}^{t_{1,i}}}{\Delta z_{\text{nose}}}\right)^2 + \left(-\frac{\delta \Delta t}{\Delta t}\right)^2 + \left(\frac{\delta h_{\text{cal.},m}}{h_{\text{cal.},m}}\right)^2 + \left(-\frac{\delta h_{\text{cal.,px}}}{h_{\text{cal.,px}}}\right)^2 \tag{18}$$

By simplifying further, one obtains:

$$\left(\frac{\delta U}{U}\right)^2 = 2\left(\frac{\delta z_{\text{nose}}}{\Delta z_{\text{nose}}}\right)^2 + \left(\frac{\delta \Delta t}{\Delta t}\right)^2 + \left(\frac{\delta h_{\text{cal.},m}}{h_{\text{cal.},m}}\right)^2 + \left(\frac{\delta h_{\text{cal.,px}}}{h_{\text{cal.,px}}}\right)^2 \tag{19}$$

where δz_{nose} refers to the uncertainty of the bubble nose vertical coordinate, regardless of the time instant. Notice that the uncertainty of the latter variable is, obviously, similar, in different time instants. A final algebraic manipulation yields an expression for the relative uncertainty of the bubble velocity variable:

$$\frac{\delta U}{U}\left[\frac{m}{m}\right] = \sqrt{2\left(\frac{\delta z_{\text{nose}}}{\Delta z_{\text{nose}}}\right)^2 + \left(\frac{\delta \Delta t}{\Delta t}\right)^2 + \left(\frac{\delta h_{\text{cal.},m}}{h_{\text{cal.},m}}\right)^2 + \left(\frac{\delta h_{\text{cal.,px}}}{h_{\text{cal.,px}}}\right)^2} \tag{20}$$

Table 1
Values of parameters and absolute uncertainties in the calculation of bubble velocity uncertainty

Parameter	Units	Value
Δz_{nose}	[pixel]	28.7
δz_{nose}	[pixel]	1
Δt	[s]	0.04
$\delta \Delta t$	[s]	1.25×10^{-4}
$h_{\text{cal},m}$	[m]	0.18
$\delta h_{\text{cal},m}$	[m]	5×10^{-4}
$h_{\text{cal,px}}$	[pixel]	221.5
$\delta h_{\text{cal,px}}$	[pixel]	2
$\delta U_B/U_B$	[$\text{ms}^{-1}/\text{ms}^{-1}$]	0.05019

Table 1 shows the values of the parameters used in the computation of the uncertainty of bubble velocity variable.

Typical values of the parameters required for the computation of uncertainty were estimated as the average values of experiments with several superficial gas and liquid velocities (ranging from 0.1 to 0.15 m/s). A typical bubble nose displacement of 28.7 pixels was considered. Moreover, 1 pixel uncertainty is considered in the determination of the bubble nose positioning (δz_{nose}; assumed equal to the maximum deviation between algorithm and operator predictions for bubble nose positioning, for a large number of frames). An image frame is grabbed every 0.04 s (25 Hz camera frequency; $\Delta t = 0.04$ s) with an uncertainty of 1.25×10^{-4} s (half of the frame exposure time: 1/4000 s; $\delta \Delta t = 0.5 \times 1/4000 = 1.25 \times 10^{-4}$ s). An 0.18 m calibration element was used with an uncertainty of 5×10^{-4} m (half of the smallest scale interval: 0.001 m). A 2 pixel uncertainty is considered in the length of the calibration element, since its borders, in the calibration image, are defined by an operator). The aforementioned data results in a 5% uncertainty in the velocity of the bubbles.

5.2. Bubble length

The following equation provides the length of bubbles as a function of the position of their boundaries (the reduction equation; based on Eqs. (2) and (5)):

$$h_{b,i} = \left(z_{\text{nose},i}^{t_{2,i}} - z_{\text{rear},i}^{t_{2,i}}\right)\frac{h_{\text{cal.},m}}{h_{\text{cal.,px}}} \Leftrightarrow h_b = (z_{\text{nose}} - z_{\text{rear}})\frac{h_{\text{cal.},m}}{h_{\text{cal.,px}}} \tag{21}$$

Following an approach similar to the one used for the bubble velocity variable, one obtains the uncertainty of h_b:

$$(\delta h_b)^2 = \left(\frac{\partial h_b}{\partial z_{\text{nose}}}\delta z_{\text{nose}}\right)^2 + \left(\frac{\partial h_b}{\partial z_{\text{rear}}}\delta z_{\text{rear}}\right)^2$$

$$\frac{\delta h_s}{h_s}\left[\frac{m}{m}\right] = \frac{\sqrt{\left(\frac{h_{\text{cal.},m}}{h_{\text{cal.,px}}}\right)^2 \left(\delta h_s\,[\text{px}]\right)^2 + \left(\frac{h_s[\text{px}]}{h_{\text{cal.,px}}}\delta h_{\text{cal.},m}\right)^2 + \left(\frac{h_s[\text{px}]h_{\text{cal.},m}}{(h_{\text{cal.,px}})^2}\delta h_{\text{cal.,px}}\right)^2}}{h_s}$$

Box I.

$$\delta h_s\,[\text{px}] = \sqrt{(\delta z_{\text{rear}})^2 + (\delta z_{\text{nose}})^2 + 2\,(U\delta t)^2 + 2\left(\frac{\Delta t_{\text{bubble}}}{\Delta t}\delta z_{\text{nose}}\right)^2 + \left(\Delta t_{\text{bubble}}\frac{\Delta z_{\text{nose}}}{\Delta t^2}\delta\Delta t\right)^2}$$

Box II.

Table 2
Values of parameters and absolute uncertainties in the calculation of bubble length uncertainty

Parameter	Units	Value
δz_{nose}	[pixel]	1
δz_{rear}	[pixel]	5
h_b	[pixel]	225.4
$\delta h_b/h_b$	[m/m]	0.0245

$$+\left(\frac{\delta h_{\text{cal.},m}}{h_{\text{cal.},m}}\right)^2 + \left(\frac{\delta h_{\text{cal.,px}}}{h_{\text{cal.,px}}}\right)^2 \tag{22}$$

which yields, after rearrangement:

$$\frac{\delta h_b}{h_b}\left[\frac{m}{m}\right] = \sqrt{\left(\frac{\delta z_{\text{nose}}}{h_b}\right)^2 + \left(\frac{\delta z_{\text{rear}}}{h_b}\right)^2 + \left(\frac{\delta h_{\text{cal.},m}}{h_{\text{cal.},m}}\right)^2 + \left(\frac{\delta h_{\text{cal.,px}}}{h_{\text{cal.,px}}}\right)^2} \tag{23}$$

Table 2 shows the values of the main parameters, considered in the computation of bubble length uncertainty.

Notice that a higher uncertainty is considered for the positioning of the rear of the bubble (5 pixels instead of 1 pixel). This figure was obtained taking the maximum deviation between algorithm and operator predictions for bubble rear positioning, for a large number of frames. A typical bubble length value of 225.4 pixels is considered (as before, the average value of several experimental conditions). These uncertainties, together with those regarding the calibration procedure, result finally in a 2.5% uncertainty in the bubble length variable.

5.3. Slug length

The length of the liquid slugs can be computed by considering simultaneously Eqs. (1)–(5):

$$h_{s,i-1} = \underbrace{\left(z_{\text{rear},i-1}^{t_{2,i-1}} - z_{\text{nose},i}^{t_{2,i}} + (t_{2,i} - t_{2,i-1})\frac{z_{\text{nose},i-1}^{t_{2,i-1}} - z_{\text{nose},i-1}^{t_{1,i-1}}}{\Delta t}\right)}_{h_s[\text{px}]} \times \frac{h_{\text{cal.},m}}{h_{\text{cal.,px}}} = h_s\,[\text{px}]\,\frac{h_{\text{cal.},m}}{h_{\text{cal.,px}}} \tag{24}$$

where h_s[px] refers to the length of the slug in pixel units. Following an approach similar to the one described in the previous sections, one obtains an expression (Box I) for the computation of the uncertainty of h_s, in real length units, where δh_s[px] refers to the uncertainty of h_s in pixel units. This parameter is calculated as in Box II, where Δt_{bubble} stands for the time interval required to have two consecutive bubble noses passing the reference line, δt is the uncertainty of variables $t_{2,i}$ and $t_{2,i-1}$ (obviously similar), and z_{rear} and z_{nose} refer to variables $z_{\text{rear},i-1}^{t_{2,i-1}}$ and $z_{\text{nose},i}^{t_{2,i}}$, respectively. Absolute uncertainties and typical parameter values, required to assess the uncertainty of slug length variable, are shown in Table 3.

Table 3
Values of parameters and absolute uncertainties in the calculation of slug length uncertainty

Parameter	Units	Value
δz_{rear}	[pixel]	5
δz_{nose}	[pixel]	1
δt	[s]	1.25E−04
$\delta\Delta t$	[s]	1.25E−04
Δt	[s]	0.04
Δt_{bubble}	[s]	1.121
Δz_{nose}	[s]	28.7
h_s	[pixel]	580.1
h_s	[m]	0.471
h_b	[pixel]	225.4
U	[pixel/s]	718.7
$\delta h_s/h_s$	[m/m]	0.0697

As with Δt, variable t has an associated uncertainty equal to half of the typical exposure time (1/4000 s; $\delta t = 0.5 \times 1/4000 = 1.25 \times 10^{-4}$ s). The uncertainties in the positioning of the bubble nose (δz_{nose}) and the bubble rear (δz_{rear}) are estimated as in the previous sections. The remaining typical parameters are estimated based on data of several experimental conditions. The aforementioned values result in a 7% uncertainty in the slug length variable.

6. Conclusions

An image analysis technique for the study of continuous co-current gas–liquid slug flow, in vertical columns, is reported. The technique allows the straightforward measurement of several slug flow characteristics with almost no input from the operator (exception: calibration procedure). A specially-built illumination kit, together with custom-made object tracking routines enable the thorough study of slug flow pattern, in

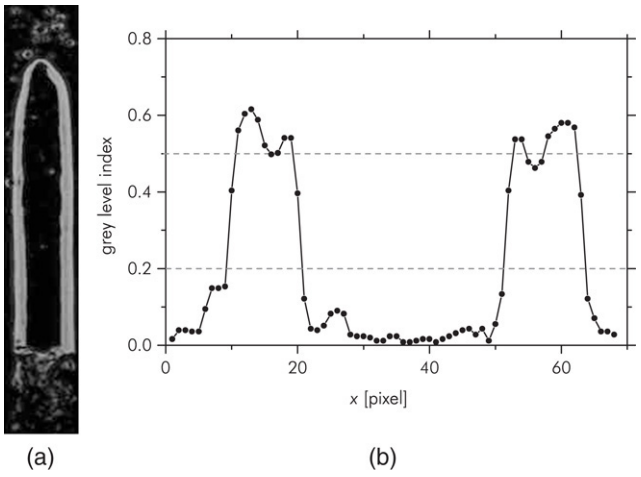

Fig. 10. (a) Experimental frame before conversion to binary mode; (b) grey level profile along a cross section of the experimental frame.

continuous operation, by informing extensively on parameters such as bubble velocity, bubble length and liquid slug length.

The evaluation of the uncertainty associated with the parameters measured with the proposed technique is performed. The *general uncertainty analysis approach* is used to assess the propagation of the partial uncertainties (in bubble boundary definition, time measurement and calibration procedure) over the mentioned flow parameters. Relative uncertainties of about 5%, 2.5% and 7% were found for bubble velocity, bubble length and liquid slug length, respectively. These low uncertainties support and advise the further implementation of image analysis techniques, as an important tool for the study of slug flow characteristics.

Acknowledgments

The authors gratefully acknowledge the financial support of Fundação para Ciência e a Tecnologia through project POCTI/EQU/33761/1999 and scholarship SFRH/BD/11105/2002. POCTI (FEDER) also supported this work via CEFT.

Appendix. On the threshold value

The conversion of a given greyscale image to binary mode requires the definition of the threshold value (see Section 3). Furthermore, the level of accuracy of the resulting binary image (i.e. the measure of how well the binary image represents the original greyscale image) is related, obviously, to the luminosity chosen for threshold. Consider Fig. 10(a) showing a frame of a slug flow experiment, right before the conversion to binary mode. The grey level profile along the middle cross-section of the frame is shown in Fig. 10(b). The bubble contour (brighter areas of the image) can easily be located in the grey level profile (two peaks of the curve). Furthermore, one can spot the gas–liquid interface by analysing the variation of the grey level index, namely around the main peaks of the profile. For instance, the gas–liquid interface can be detected by the steep variation of the grey level index, from about 0.2 to about 0.5 (Fig. 10(b)). It is interesting, however, to assess the sensitivity of the measured parameters (U, h_b and h_s) to the threshold value. For that purpose a sensitivity test was performed in which those parameters were obtained for a set of 10 Taylor bubbles, using different threshold values (0.25, 0.35 and 0.45). The parameters obtained were compared statistically, the results of which are shown, in brief, in Table 4. The estimates of each measured parameter, obtained using the different thresholds, are fairly similar. Moreover, the standard deviation of the different estimates reaches about 1.2%, 1.3% and 1.9% of the corresponding average (for U, h_b and h_s, respectively; see Table 4). This indicates that the estimates of these parameters are not particularly sensitive to the threshold value chosen for the binary conversion procedure, as long as it is in the range 0.25–0.45. As mentioned in Section 3, a threshold value of 0.35 was used for most experiments.

Table 4
Standard deviation of the estimates of bubble velocity, bubble length and liquid slug length, obtained using threshold values of 0.25, 0.35 and 0.45 (for ensemble of 10 Taylor bubbles)

Parameter	Stand. dev. [% of avg.]
U	1.2
h_b	1.3
h_s	1.9

References

[1] Pinto AMFR, Coelho Pinheiro MN, Campos JBLM. On the interaction of Taylor bubbles rising in two-phase co-current slug flow in vertical columns: Turbulent wakes. Experiments in Fluids 2001;31(6):643–52.
[2] Van Hout R, Barnea D, Shemer L. Evolution of statistical parameters of gas–liquid slug flow along vertical pipes. International Journal of Multiphase Flow 2001;27(9):1579–602.
[3] Hasanein HA, Tudose GT, Wong S, Malik M, Esaki S, Kawaji M. Slug flow experiments and computer simulation of slug length distribution in vertical pipes. AIChE Symposium Series 1996;92(310):211–9.
[4] Polonsky S, Shemer L, Barnea D. The relation between the Taylor bubble motion and the velocity field ahead of it. International Journal of Multiphase Flow 1999;25:957–75.
[5] Van Hout R, Barnea D, Shemer L. Translational velocities of elongated bubbles in continuous slug flow. International Journal of Multiphase Flow 2002;28(8):1333–50.
[6] Sousa RG, Pinto AMFR, Campos JBLM. Effect of gas expansion on the velocity of a Taylor bubble: PIV measurements. International Journal of Multiphase Flow 2006;32:1182–90.
[7] The MathWorks, I. Help files of "MATLAB: The language of technical computing". 2002.